

RSC Advances



This is an *Accepted Manuscript*, which has been through the Royal Society of Chemistry peer review process and has been accepted for publication.

Accepted Manuscripts are published online shortly after acceptance, before technical editing, formatting and proof reading. Using this free service, authors can make their results available to the community, in citable form, before we publish the edited article. This *Accepted Manuscript* will be replaced by the edited, formatted and paginated article as soon as this is available.

You can find more information about *Accepted Manuscripts* in the [Information for Authors](#).

Please note that technical editing may introduce minor changes to the text and/or graphics, which may alter content. The journal's standard [Terms & Conditions](#) and the [Ethical guidelines](#) still apply. In no event shall the Royal Society of Chemistry be held responsible for any errors or omissions in this *Accepted Manuscript* or any consequences arising from the use of any information it contains.



Failure of multi-layer graphene coatings in acidic media

F. Yu, A. C. Stoot, P. Bøggild and L. Camilli*

Received 00th January 20xx,
Accepted 00th January 20xx

DOI: 10.1039/x0xx00000x

www.rsc.org/

Being impermeable to all gases, graphene has been proposed as an effective ultrathin barrier film and protective coating. However, here it is shown how the gastight property of graphene-based coatings may indirectly lead to their catastrophic failure under certain conditions. When nickel coated with a thick, high-quality chemical vapor deposited multilayered graphene is exposed to acidic solutions, a dramatic evolution of gas is observed at the coating-substrate interface. The gas bubbles grow and merge, eventually rupturing and delaminating the coating. This behavior, attributed to cathodic hydrogen evolution, can also occur spontaneously on a range of other technologically important metals and alloys based on iron, zinc, aluminum and manganese; this making these findings relevant for practical applications of graphene-based coatings.

Introduction

Corrosion, the gradual degradation of metals and alloys by interaction with the environment, is a problem of enormous significance. Costs due to corrosion represent 3-4% of the worldwide BNP.¹ Corrosion and oxidation cause waste of valuable resources, loss or contamination of product, reduction in efficiency and costly maintenance across many industries. Moreover, failure of critical metal parts is not just expensive, but potentially dangerous. Passivating and protective coatings comprise a widely applied approach to improve surface properties of substrates and to protect materials from environmental degradation. To this aim, efficiently separating the substrate from the external environment is one of the most critical functions of a protective coating.

The hexagonal lattice of defect-free monolayer graphene has been proved both theoretically and experimentally to be impermeable to all liquids and gases including the smallest molecules, hydrogen and helium.²⁻⁴ This outstanding feature has led to an enormous interest in employing graphene as an anticorrosion coating for metals and alloys.⁵⁻⁷ Nevertheless, chemical vapour deposited (CVD) monolayer graphene generally exhibits defects through which molecules and radical species can diffuse, thus locally initiating metal corrosion.⁸⁻¹⁰ In addition, it has been reported that once these local corrosion processes begin to take place underneath a monolayer graphene cover, they are actually even accelerated by the

presence of graphene itself.¹¹ In this context, using a film made of several layers instead of a monolayer is one logical approach to improve performance of graphene-based protective coatings.¹²⁻¹⁴ In this work, however, we report a so far unnoticed issue related to coatings with low permeability and high structural integrity. Indeed, when nickel coated with a thick, high-quality multi-layered graphene is immersed in an acidic solution, the cathodic reaction spontaneously yields hydrogen at the nickel surface. The formed gas is not able to escape the high quality regions of the graphene film and therefore remains trapped and eventually forms bubbles, which can even lead to the delamination of the whole coating.

Experimental

Growth, transfer and characterization of MLG

Nickel foil (part No. 12722 from Alfa Aesar) was acetone ultrasonicated before graphene growth. Atmospheric pressure CVD growth was conducted with an AS-ONE CVD system from Annealsys. After loading the samples into the growth chamber, the chamber was evacuated with a rotary pump and then flushed with Ar three times before finally filling it up to atmospheric pressure. Next, the samples were heated at 950 °C for 15min under the co-flow of 120 sccm and 100 sccm of Ar and H₂, respectively. The growth process was then carried out for 5min at 950 °C with 2 sccm C₂H₂ and 100 sccm H₂. Lastly, the chamber was cooled down with a rate of 20 °C/s after the pressure was pumped down below 5 mbar.

Transfer of graphene coating onto glass slide or ~88 nm SiO₂ wafer was carried out via chemical etching of nickel in 5% HCl and 30% H₂O₂ mixed solution for 24 hours.

Optical images were taken with a Nikon Eclipse L200N optical microscope, while Raman spectra were collected by a Thermo

^a Technical University of Denmark, Department of Micro- and Nanotechnology, Kgs. Lyngby, DK-2800, Denmark.

* lcam@nanotech.dtu.dk

Electronic Supplementary Information (ESI) available: polarization curves, electrochemical impedance spectroscopy, further Raman characterizations of the coating and the video of the real-time microscope experiments. See DOI: 10.1039/x0xx00000x

Fisher Scientific DXR Raman microscope (excitation wavelength 455nm). Quanta 200 FEG environmental scanning electron microscope (SEM) and FEI Titan T20 G2 transmission electron microscope (TEM) were employed for the electron microscopy characterizations.

Electrochemical measurements

Polarization curves and electrochemical impedance spectroscopy (EIS) measurements were carried out with a three-electrode cell, using a AgCl/Ag reference electrode, a Pt foil as a counter electrode and a working electrode of tested samples, with a solution of 0.5M HCl (aq) being the electrolyte. All measurements were repeated on three samples in a Faraday cage using a Gamry Reference 3000 potentiostat. Polarization curves were obtained after one hour of immersion by sweeping the potential from -300mV to 300mV vs the open circuit potential (OCP) with a scan rate of 0.5 mV/s. EIS spectra were collected by applying a ± 10 mV sinusoidal perturbation (vs OCP) on tested samples at a frequency range from 100,000Hz to 0.01Hz with 10 points per decade.

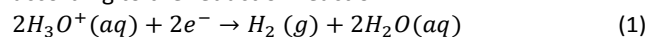
Real-time microscopy experiments of hydrogen formation below the MLG coating

The *real-time* microscopy experiments were performed with a Nikon Eclipse L200N optical microscope and a Helios Nano Lab electron microscope. In both cases, the samples were exposed to 0.5M HCl (aq) solution. The reader can refer to the next paragraph for more details of the performed *real-time* experiments.

Results and discussion

Figure 1a reports an example of the bare nickel foil and the nickel foil coated with a CVD grown multilayered graphene (MLG) film, which have been the subject of this study. The MLG film is hydrophobic with a measured static water contact angle of $102.0^\circ \pm 0.4^\circ$, and floats as a monolithic piece on water after nickel being chemically etched (Figure 1b), even though it is more than twice as dense as water. Raman spectroscopy provides information about the stacking order of the MLG¹⁵ film and the density of defects.¹⁶ For our samples, we find both AB-stacked and turbostratic regions (blue and red curve in Figure 1c, respectively), with a higher prevalence of the former case, as expected for CVD graphene.¹⁷ Regarding defect density, the small D-peak to G-peak ratio (0.040 ± 0.010) is the hallmark of the high quality film in terms of structural defects. X-ray diffraction analysis reveals an average interlayer distance of $\sim 3.3\text{\AA}$ (See Supplementary information). The cross-sectional transmission electron micrograph (TEM) displayed in Figure 1d gives insight into the total thickness of the MLG film (around 100 nm) and highlights the constant interlayer distance of the film, as shown by the Fourier Transform displayed in the Inset.

Nickel and its alloys are usually corrosion resistant in neutral, alkaline and diluted acidic media, while they deteriorate in aerated aggressive acidic environment. Hence, to investigate the corrosion performance of MLG coatings on nickel, we employ standard potentiodynamic polarization technique in 0.5M HCl solution (pH= 0.3). With this method, by sweeping potential from negative to positive values with respect to the open circuit potential, the sample is electrochemically polarized, which allows us to obtain information about thermodynamics (i.e., corrosion potential) and kinetics (i.e., corrosion current density and corrosion rate) of the corrosion process.¹⁸ Here, we estimate that the corrosion rate for the MLG-coated nickel is less than half that of the bare nickel specimen (see Supplementary Info for more details). This trend is also confirmed by electrochemical impedance spectroscopy analysis (see Supplementary Info) and is in agreement with previous studies on coatings based on few-layer graphene on nickel.¹⁹ During the test, as expected, we could notice formation of hydrogen bubbles on the surface of both samples at the cathodic branch of the polarization curves (Figure 2a), according to the reduction reaction:



We further investigated the specimen surface by means of scanning electron microscopy (SEM). In Figure 2b we report an example of an area where the MLG coating was locally delaminated. The approximately circular shape of the hole in the coating suggests that it has been caused upon rupture of a hydrogen bubble. However, the outward direction of the remaining MLG flakes at the surface near the edges of the hole suggests that the bubble was not located on the surface of the coating, but rather at the interface between it and the nickel substrate.

The formation of hydrogen bubbles at the interface between coating and substrate in aggressive acid environment is a known phenomenon in corrosion science.^{20,21} Also, it is worth reminding that, though under different conditions, the evolution of hydrogen bubbles at the interface between graphene and metal substrate during the cathodic reaction is a method largely used for graphene transfer.²²

To investigate whether the hydrogen bubbles are being generated both at the surface of the MLG film and underneath, we applied a fixed negative potential (-0.6V vs Ag/AgCl) to the coated nickel sample in 0.5 M HCl solution for only a short period of time (3 min). In this way, the bubbles can be observed at the interface before they become large enough to burst. As soon as the potential was applied, numerous hydrogen bubbles appeared at the surface of the coating. After this test, the sample was rinsed with water and gently blow-dried with nitrogen. Under the optical microscope, a few nearly circular protrusions of approximately 20 μm in diameter were found at seemingly un-correlated locations under the graphitic film. To prove that these protrusions are actually blisters, i.e. trapped gas underneath the graphene film and not particles or contaminants present on the surface, we characterized these structures by scanning electron microscopy. Figure 2c displays two such protrusions that

indeed seem to be blisters of the coating. Notably, the characteristic graphene wrinkles²³ at the base of the blisters gradually unfold near the center of the blister, as would be expected. To demonstrate that these blisters can become large enough to burst and locally delaminate the coating, we apply a fixed negative potential (-0.6V vs Ag/AgCl) to the coated nickel sample in 0.5M HCl solution for 30 min. As displayed in Figure 2d, SEM analysis shows that in many places, the coating is no longer covering the metal substrate, similar to what was found after the potentiodynamic scan experiment, which is another indication that the film has now ruptured and delaminated. Raman spectroscopy was also used to prove that no graphene is present in the delaminated areas (see Supplementary information).

Raman spectroscopy is also known to provide information regarding mechanical stress in the graphene lattice. A significant blue-shift of all the peaks in the spectrum has been indeed reported for the case of micro-balloons made of single and bi-layer graphene on a oxidized silicon substrate.²⁴ However, within our samples, we do not observe any remarkable shift of the peaks in the Raman spectra either recorded at the center of the blister, at its base, or away from the blister on a flat graphene region (see Supplementary information). This can be understood looking at Figure 2c, where the wrinkles seem to unfold at the center of the blister, thereby relieving any stress caused by the trapped hydrogen. The wrinkles are naturally formed upon cooling after the growth process as a consequence of the different thermal expansion coefficients of graphene and nickel;²³ likewise the unfolding of wrinkles is a way to release the mechanical stress caused by the formation of the blisters.

To gain more insights into the formation of the hydrogen bubbles below the MLG film, we set up two experiments for real-time monitoring of the process. The first experiment consists of placing a droplet of 0.5 M HCl solution in the center of the MLG-coated Ni foil under an optical microscope. Already after 5 min, few blisters can be seen randomly distributed over the imaged area, initially with diameters ranging from 10 μm to 20 μm (Figure 3a). These blisters grow over time due to a build-up of hydrogen at the interface between nickel and the coating until they eventually start to merge. This behavior continues as long as the HCl droplet is present on top of the MLG film. After two hours the blisters can be larger than 100 μm and locally lift up the coating (Figure 3a). It is worth noticing that the time scale for hydrogen bubble formation actually varies depending on the sample under study. Interestingly, once the acid droplet is removed, the region of the sample under the droplet does not seem to be visibly corroded, i.e. there is no noticeable change in color or appearance. On the other hand, the region of the sample surrounding the droplet, which is thus not in immediate contact with the acid, exhibits remarkable signs of degradation (see Figure 3b and Figure 3c, respectively). If the acid is distributed all over the sample area, the blisters eventually cause delamination of the whole coating (see Supplementary information).

In the second experiment, SEM is used in order to study the hydrogen bubble formation in real-time with higher spatial resolution. A droplet of 0.5 M HCl solution is placed in the center of the MLG-coated nickel foil, and gently removed with a tissue. The sample is mounted inside the scanning electron microscope without prior rinsing or blow-drying. When the electron beam is focused on a flat region of the sample, a dramatic hydrogen evolution takes place below the MLG film (Figure 4).

At first, a single micrometer-size blister is observed, then, other smaller blisters are formed all over the scanned area (Figure 4b and Figure 4c, respectively). At lower magnification, it is possible to see that the blister-like protrusions are mainly found in the area that was initially irradiated by the scanning electron beam (see Supplementary Materials). This might be explained by a monolayer of the acidic solution still being adsorbed on the surface²⁵ as well as within defects and crevices of the MLG film after the sample has being placed inside the microscope and evacuated. Then, the local heating and the creation of defects²⁶ induced by the electron beam trigger and accelerate the diffusion of water through the MLG coating thus giving rise to the hydrogen bubble formation. This experiment points out that (i) the fact that such gas evolution only occurs with samples that have been exposed to HCl solution rules out that this phenomenon is caused by the presence of residual gas trapped either between graphene and nickel or into the nickel itself during the CVD process; and (ii) the trapping of gas at the graphene-metal interface in vacuum conditions inside the SEM chamber indicates that the overall quality and integrity of the film is high, as also corroborated by Raman spectroscopy investigation (see Figure 1c).

To explain why hydrogen is formed at the interface, we suggest that, even if few, local defects and inhomogeneities are intrinsically present in the coating. Notably, such inhomogeneities are areas with higher defect density, grain boundaries,^{27, 28} and sometimes also fewer layers (see Supplementary Information). These areas may originate from local impurities on the nickel surface, temperature gradients during the synthesis process or different catalytic activity of the nickel grains, as already reported in the literature for CVD grown multilayer graphene.²⁹ In this scenario, as the coating is placed in contact with the acidic solution, water fills these defects and inhomogeneities thus forming a bridge which allows protons to shuttle from outside the coating to the nickel surface, through the hydrogen-bonding network (Figure 5), similar to the case of proton transport through the channel of carbon nanotubes.^{30, 31} As water reaches the nickel, the cathodic reaction locally takes place. In fact, as described by the potential-pH diagram of nickel/water system, also known as Pourbaix diagram,³² the evolution of hydrogen at the nickel-water interface is spontaneous at the low pH level used in this study. As the MLG coating on nickel shifts the open circuit potential of nickel by only -25 mV (see Supplementary Info), the hydrogen evolution process for the MLG-coated nickel is still spontaneous, in accordance with our observations. Once hydrogen is formed at the coating-metal interface, we can

assume it diffuses on the nickel surface, as observed in similar systems,³³ and merge, thus giving rise to the observed blisters. Since the majority of the coating is made of regions with very small apparent density of defects, a build-up of hydrogen occurs under the MLG film, produces bubbles that grow and merge, and eventually delaminate the coating. The formed hydrogen is not likely to pass through the coating via local defects and inhomogeneities, since these are clogged by water molecules, as previously suggested for helium-leak-tight coatings made of graphene oxide.³⁴ The fact that the formation of hydrogen bubbles takes place on a different time scale depending on the sample under study could be explained by varying density of inhomogeneous areas within the coating, which is easily accountable by variations of the nickel foil substrates or inevitable differences in the exact growth conditions commonly experienced for CVD graphene growth. Here, it is worth pointing out that proton transport through a defect-free single layer of graphene has already been observed, but not through a bilayer.³⁵ In this study we study the performance of a coating comprised of hundreds of graphene layers, and therefore cannot immediately adopt the explanation proposed by Hu and co-workers,³⁵ where a tunnel mechanism was invoked.

The dramatic degradation of the sample in the regions surrounding the acid droplets can be ascribed to the formation of a galvanic cell between nickel and graphene. Every electrochemical reaction consists of a cathodic and an anodic part. In the case of the acid droplet deposited on the middle of the MLG-coated sample, the cathodic reaction (i.e., reduction of protons to hydrogen) occurs under the droplet due to the abundance of protons, while the anodic one (i.e., oxidation of the nickel) takes place away from the droplet. While reducing protons to hydrogen, electrons are being continuously depleted in the region under the droplets. In this picture, electrons will move from the region surrounding the droplet, to the region below the droplet in compensation. Here, as already reported in the case of single layer graphene grown on copper foil,¹¹ the electrons may migrate through the graphene film due to its high conductivity, rather than through the passivated metal surface, thus giving rise to formation of a galvanic cell which spreads the oxidation of nickel to all regions in contact with graphene.

Ultimately, in order to verify that the formation of hydrogen beneath a graphene coating is a reaction occurring spontaneously in the system nickel/water at low pH values, regardless of the anions that are present in solution, we repeat the experiment of the droplet placed at the center of the coated substrate using different acids. At this aim, a MLG-coated nickel foil is cut into three pieces. The first piece is tested with HCl, the second one with H₂SO₄ whereas the third one with HNO₃, all solutions being at the same concentration (namely 0.5M). As displayed in Figure 6, after 240min of exposure, the coating results in being lifted up in several areas by hydrogen in all the three cases, regardless of the acids that was used.

Conclusions

Our observations show that protective coatings based on CVD MLG might fail in certain chemical environments. Even for MLG consisting of hundreds of layers, with nominally very few defects, the few but inevitable inhomogeneities provide sufficient pathways for acid to reach the Ni surface, where hydrogen is spontaneously formed. We suggest that the very integrity and quality of the MLG coating prevents excess gas to escape at a rate that matches the rate of which it is formed, which thus leads to hydrogen build-up and eventually catastrophic delamination to the coating. This implies that coatings based on graphene and other two-dimensional materials, which are considered attractive for corrosion protection due to their impermeability, may fail for the same reason. Notably, the vulnerability to gas evolution below the coating may become increasingly severe as the thickness, quality and homogeneity of the coating is improved, as this will prevent gas from escaping in a non-destructive manner. Our findings may be relevant for other electrochemically active metals and alloys made for instance of iron, zinc, manganese and aluminium.

On the other hand, however, it is also worth pointing out that (i) the possibility of spontaneously producing and effectively trapping hydrogen (or other gases) calls for further investigations of such MLG film in fields such as gas storage and production; and (ii) the capability of such membranes of being selectively permeable to water might be of great interest for particular environmental applications.³⁶

Acknowledgements

The authors are grateful to Dr. Rahul Raveendran Nair and Jijo Abraham for providing the XRD data and for the useful discussions. The authors also thank Dr. David Mackenzie for help with the analysis of Raman data.

This project was supported by The Strategic Danish Research collaboration (DSF) with the DA-GATE project (12-131827) and through the high technology foundation (HTF) with the NIAGRA project (058-2012-4). L.C. thanks funding support from The Danish Council for Independent Research | Technology and Production Sciences (FTP) through the Mobilex grant 'Atomically thin coatings'.

Notes and references

1. A. El-Meligi, *Recent Patents on Corrosion Science*, 2010, **2**, 22-33.
2. J. S. Bunch, S. S. Verbridge, J. S. Alden, A. M. van der Zande, J. M. Parpia, H. G. Craighead and P. L. McEuen, *Nano Lett.*, 2008, **8**, 2458-2462.
3. O. Leenaerts, B. Partoens and F. M. Peeters, *Appl. Phys. Lett.*, 2008, **93**, 193107.
4. M. Miao, M. B. Nardelli, Q. Wang and Y. Liu, *PCCP* 2013, **15**, 16132-16137.

5. S. Chen, L. Brown, M. Levendorf, W. Cai, S.-Y. Ju, J. Edgeworth, X. Li, C. W. Magnuson, A. Velamakanni and R. D. Piner, *ACS nano*, 2011, **5**, 1321-1327.
6. D. Prasai, J. C. Tuberquia, R. R. Harl, G. K. Jennings and K. I. Bolotin, *ACS nano*, 2012, **6**, 1102-1108.
7. N. T. Kirkland, T. Schiller, N. Medhekar and N. Birbilis, *Corros. Sci.*, 2012, **56**, 1-4.
8. D. L. Duong, G. H. Han, S. M. Lee, F. Gunes, E. S. Kim, S. T. Kim, H. Kim, Q. H. Ta, K. P. So, S. J. Yoon, S. J. Chae, Y. W. Jo, M. H. Park, S. H. Chae, S. C. Lim, J. Y. Choi and Y. H. Lee, *Nature*, 2012, **490**, 235-239.
9. I. Wlasny, P. Dabrowski, M. Rogala, P. J. Kowalczyk, I. Pasternak, W. Strupinski, J. M. Baranowski and Z. Klusek, *Appl. Phys. Lett.*, 2013, **102**, 111601.
10. Y.-P. Hsieh, M. Hofmann, K.-W. Chang, J. G. Jhu, Y.-Y. Li, K. Y. Chen, C. C. Yang, W.-S. Chang and L.-C. Chen, *ACS nano*, 2013, **8**, 443-448.
11. M. Schriver, W. Regan, W. J. Gannett, A. M. Zaniewski, M. F. Crommie and A. Zettl, *ACS nano*, 2013, **7**, 5763-5768.
12. N.-W. Pu, G.-N. Shi, Y.-M. Liu, X. Sun, J.-K. Chang, C.-L. Sun, M.-D. Ger, C.-Y. Chen, P.-C. Wang, Y.-Y. Peng, C.-H. Wu and S. Lawes, *J. Power Sources* 2015, **282**, 248-256.
13. A. C. Stoot, L. Camilli, S.-A. Spiegelhauer, F. Yu and P. Bøggild, *J. Power Sources* 2015, **293**, 846-851.
14. Y. Su, V. G. Kravets, S. L. Wong, J. Waters, A. K. Geim and R. R. Nair, *Nat Commun*, 2014, **5**, 4843.
15. R. Rao, R. Podila, R. Tsuchikawa, J. Katoch, D. Tishler, A. M. Rao and M. Ishigami, *ACS nano*, 2011, **5**, 1594-1599.
16. A. Eckmann, A. Felten, A. Mishchenko, L. Britnell, R. Krupke, K. S. Novoselov and C. Casiraghi, *Nano Lett.*, 2012, **12**, 3925-3930.
17. A. W. Tsen, L. Brown, R. W. Havener and J. Park, *Acc. Chem. Res.*, 2013, **46**, 2286-2296.
18. C. Lefrou, R. P. Nogueira, F. Huet and H. Takenouti, in *Shreir's Corrosion*, Elsevier, Oxford, 2010, pp. 13-51.
19. X. H. Ye, F. Yu, M. Curioni, Z. Lin, H. J. Zhang, H. W. Zhu, Z. Liu and M. L. Zhong, *RSC Adv.*, 2015, **5**, 35384-35390.
20. M. L. White, H. Vedage, R. D. Granata and H. Leidheiser Jr, *Ind. Eng. Chem. Res.*, 1986, **25**, 129-132.
21. H. Leidheiser Jr and M. W. Kendig, *Ind. Eng. Chem. Res.*, 1978, **17**, 54-55.
22. L. Gao, W. Ren, H. Xu, L. Jin, Z. Wang, T. Ma, L.-P. Ma, Z. Zhang, Q. Fu and L.-M. Peng, *Nat. Commun.*, 2012, **3**, 699.
23. S. J. Chae, F. Güneş, K. K. Kim, E. S. Kim, G. H. Han, S. M. Kim, H.-J. Shin, S.-M. Yoon, J.-Y. Choi, M. H. Park, C. W. Yang, D. Pribat and Y. H. Lee, *Adv. Mater.*, 2009, **21**, 2328-2333.
24. J. Zabel, R. R. Nair, A. Ott, T. Georgiou, A. K. Geim, K. S. Novoselov and C. Casiraghi, *Nano Lett.*, 2012, **12**, 617-621.
25. D. Chakarov, L. Österlund and B. Kasemo, *Vacuum*, 1995, **46**, 1109-1112.
26. J. Jones, P. Ecton, Y. Mo and J. Perez, *Appl. Phys. Lett.*, 2009, **95**, 246101.
27. S. C. O'Hern, C. A. Stewart, M. S. Boutilier, J.-C. Idrobo, S. Bhaviripudi, S. K. Das, J. Kong, T. Laoui, M. Atieh and R. Karnik, *Acs Nano*, 2012, **6**, 10130-10138.
28. M. S. Boutilier, C. Sun, S. C. O'Hern, H. Au, N. G. Hadjiconstantinou and R. Karnik, *ACS nano*, 2014, **8**, 841-849.
29. A. Reina, X. Jia, J. Ho, D. Nezich, H. Son, V. Bulovic, M. S. Dresselhaus and J. Kong, *Nano Lett.*, 2009, **9**, 30-35.
30. C. Dellago, M. M. Naor and G. Hummer, *Phys. Rev. Lett.*, 2003, **90**, 105902.
31. D. J. Mann and M. D. Halls, *Phys. Rev. Lett.*, 2003, **90**, 195503.
32. M. Pourbaix and R. W. Staehle, in *Lectures on Electrochemical Corrosion*, Springer, 1973, pp. 83-183.
33. E. Stolyarova, D. Stolyarov, K. Bolotin, S. Ryu, L. Liu, K. Rim, M. Klima, M. Hybertsen, I. Pogorelsky and I. Pavlishin, *Nano Lett.*, 2008, **9**, 332-337.
34. R. Nair, H. Wu, P. Jayaram, I. Grigorieva and A. Geim, *Science*, 2012, **335**, 442-444.
35. S. Hu, M. Lozada-Hidalgo, F. C. Wang, A. Mishchenko, F. Schedin, R. R. Nair, E. W. Hill, D. W. Boukhvalov, M. I. Katsnelson, R. A. Dryfe, I. V. Grigorieva, H. A. Wu and A. K. Geim, *Nature*, 2014, **516**, 227-230.
36. F. Perreault, A. Fonseca de Faria and M. Elimelech, *Chem. Soc. Rev.*, 2015, **44**, 5861-5896.

Figures

Figure 1

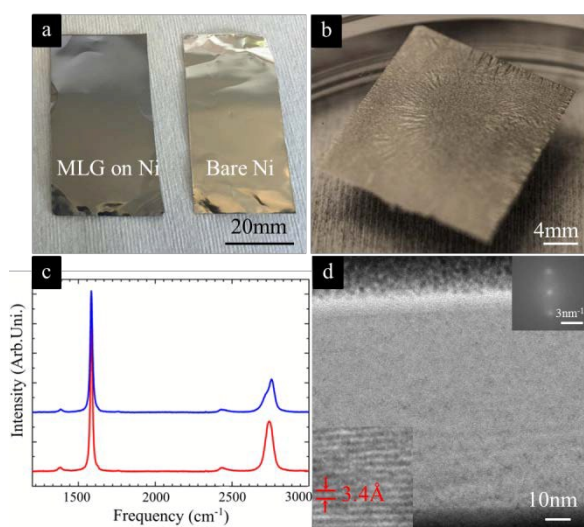


Figure 1 - (a) Multilayer graphene-coated (on the left) and bare (on the right) nickel foils. (b) Snapshot of the graphitic membrane floating on water after nickel substrate being chemically etched. (c) Two typical Raman spectra of the graphitic film showing the coexistence of regions with AB-stacking (top, blue curve) and turbostratic stacking (bottom, red curve). (d) Cross-section transmission electron microscope micrograph of the graphitic film on Ni foil. Insets: Fourier transform (top right corner) and high-resolution image (bottom left corner) both illustrating the high graphitization degree of the MLG film.

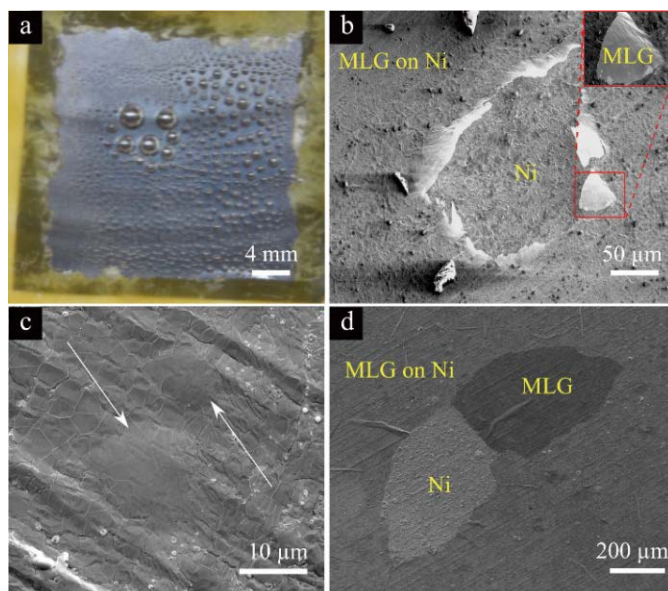


Figure 2 - (a) Snapshot of the MLG-coated nickel sample while being tested by potentiodynamic scanning at negative applied voltage (cathodic branch). Hydrogen bubbles can be observed on the surface of the sample. (b) SEM micrograph of the MLG-coated nickel foil after potentiodynamic scanning. At the center of the picture, the coating has been delaminated probably by a bursting hydrogen bubble; broken edges of the coating are now pointing outwards, suggesting that the burst bubble was located at the coating/substrate interface (inset). (c) SEM image of two bubbles – highlighted by the white arrows – found under the coating after applying constant negative potential (-0.6V vs Ag/AgCl) for 3 min to the MLG-coated nickel foil in 0.5 M HCl solution. (d) A portion of the MLG coating has been delaminated after 30 min of constant exposure to a potential of -0.6 V in 0.5M HCl solution and still lies on the sample surface

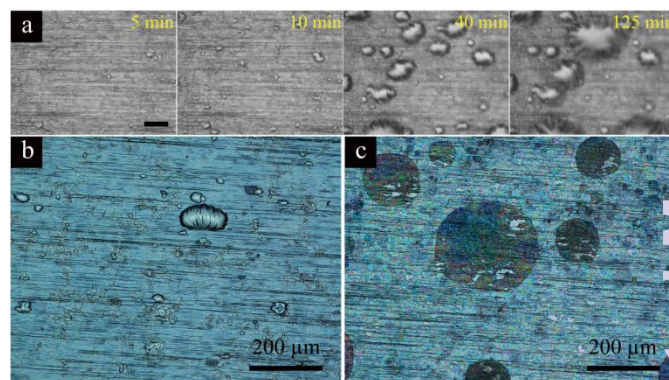


Figure 3 - (a) Sequence of optical microscope images taken from a MLG-coated nickel foil with a droplet of 0.5M HCl solution on top. The pictures are recorded through the acid droplet – hence the low quality of the images. The scale bar is 100 μm . (b, c) Optical images of an area under the acid droplet (c) and away from it (c). The sample represented in (a) is different from the one reported in (b) and (c).

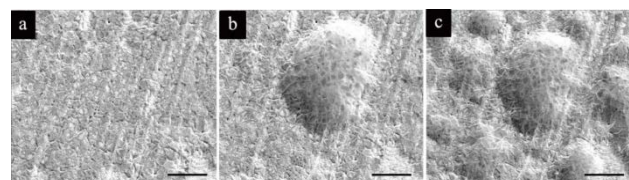


Figure 4 - Consecutive SEM micrographs recorded on a MLG-coated nickel foil after a droplet of 0.5M HCl has been placed on top and subsequently removed. The formation of hydrogen blisters over time is reported. The scale bar is 20 μm .

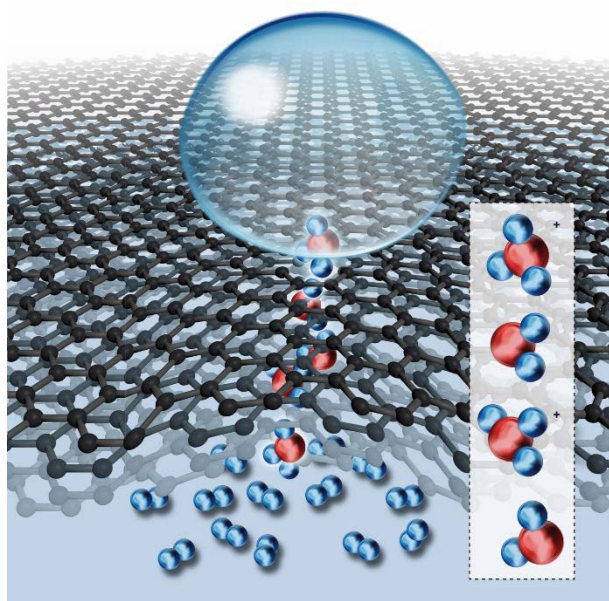


Figure 5 - Drawing of the proposed mechanism for hydrogen formation under a droplet of 0.5M HCl solution. Once the solution reaches the nickel surface through defective areas in the coating, protons – which are carried by water molecules via the Grotthuss mechanism, jumping from a molecule to the next one (inset) – are spontaneously reduced to hydrogen. The red balls represent oxygen atoms, while the blue balls stand for hydrogen atoms.

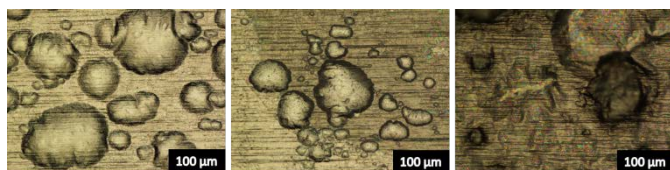
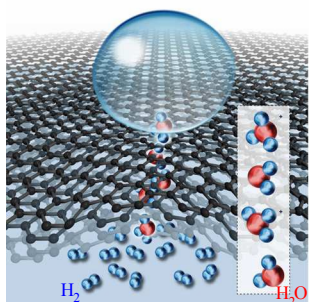


Figure 6 - Optical micrograph of three MLG-coated nickel foils exposed for 240min to 0.5M HCl (left picture), 0.5M H₂SO₄ (center picture) and 0.5M HNO₃ (right picture). In all cases, the MLG coating has been lifted in several areas due to evolution of hydrogen at the nickel-coating interface.



A new failure mechanism for high-quality multilayer graphene coatings in acidic media is described